Experimental study of bound states in ^{12}Be through low-energy ^{11}Be(d, p)-transfer reactions

J. G. Johansen,[1,2] V. Bildstein,[3] M. J. G. Borge,[4,5] M. Cubero,[5] J. Diriken,[6,7] J. Elseviers,[6] L. M. Fraile,[8] H. O. U. Fynbo,[1]
L. P. Gaffney,[9] R. Gernhäuser,[10] B. Jonson,[11] G. T. Koldste,[1] J. Konki,[4,12,*] T. Kröll,[2] R. Krücken,[10,13] D. Mücher,[10]
T. Nilsson,[11] K. Nowak,[10] J. Pakarinen,[4,12,*] V. Pesudo,[5] R. Raabe,[6] K. Riisager,[1] M. Seidlitz,[14] O. Tengblad,[5]
H. Törnqvist,[4,11] D. Voulot,[4] N. Warr,[14] F. Wenander,[4] K. Wimmer,[10,15] and H. De Witte[6]

[1]*Department of Physics and Astronomy, Aarhus University, DK-8000 Aarhus C, Denmark*
[2]*Institut für Kernphysik, Technische Universität Darmstadt, D-64289 Darmstadt, Germany*
[3]*Department of Physics, University of Guelph, Guelph, Ontario N1G 2W1, Canada*
[4]*CERN, CH-1211 Genève, Switzerland*
[5]*Instituto de Estructura de la Materia, CSIC, E-28006 Madrid, Spain*
[6]*Instituut voor Kern- en Stralingsfysica, KU Leuven, 3001 Leuven, Belgium*
[7]*Belgian Nuclear Research Centre SCK·CEN, Boeretang 200, B-2400 Mol, Belgium*
[8]*Grupo de Fisica Nuclear, Universidad Complutense, CEI Moncloa, E-28040 Madrid, Spain*
[9]*Oliver Lodge Laboratory, University of Liverpool, Liverpool L69 7ZE, United Kingdom*
[10]*Physik Department E12, Technische Universität München, 85748 Garching, Germany*
[11]*Fundamental Fysik, Chalmers Tekniska Högskola, S-41296 Göteborg, Sweden*
[12]*Helsinki Institute of Physics, P.O. Box 64, FI-00014 Helsinki, Finland*
[13]*TRIUMF, Vancouver, British Columbia V6T 2A3, Canada*
[14]*Institut für Kernphysik, Universität zu Köln, D-50937 Köln, Germany*
[15]*Department of Physics, Central Michigan University, Mount Pleasant, Michigan 48859, USA*

The bound states of ^{12}Be have been studied through a ^{11}Be(d, p)^{12}Be transfer reaction experiment in inverse kinematics. A 2.8 MeV/u beam of ^{11}Be was produced using the REX-ISOLDE facility at CERN. The outgoing protons were detected with the T-REX silicon detector array. The MINIBALL germanium array was used to detect gamma rays from the excited states in ^{12}Be. The gamma-ray detection enabled a clear identification of the four known bound states in ^{12}Be, and each of the states has been studied individually. Differential cross sections over a large angular range have been extracted. Spectroscopic factors for each of the states have been determined from distorted wave Born approximation (DWBA) calculations and have been compared to previous experimental and theoretical results.

I. INTRODUCTION

The structure of light neutron-rich nuclei has presented many challenges during the last decades [1], and this area of the nuclear chart is a prime region for investigations of halos [2–4], cluster states [5], unbound systems [6,7], as well as the vanishing of shells [8]. A key question in these topics is the spectroscopic composition of the bound states, which can be accessed experimentally in complementary ways [9–11]. We are here concerned with the structure of the bound states in ^{12}Be. The states are probed via transfer reactions. This method has recently been employed also for the study of other exotic nuclei [12–14]. In neither of the neighboring isotopes ^{11}Li and ^{11}Be can the ground states be written as a simple single-particle configuration (see [15] and the references above). This seems to also be the case for ^{12}Be.

Four bound states are presently known in ^{12}Be; see Fig. 1. The highest lying bound state (1_1^-) has an excitation energy of only $E^* = 2.70$ MeV. Hence the level density in ^{12}Be is relatively high for a light nucleus; in comparison the first excited states in ^{10}Be and ^{13}B have an excitation energy above

3 MeV and in ^{12}C the first excited state is at 4.4 MeV. This high level density is believed to be due to configurations from both the $0p_{1/2}$ shell and the $1s_{1/2}0d_{5/2}$ shell, a situation which is also known to occur in ^{11}Be [16]. The configuration mixing was first suggested in 1976 by Barker [17] following a β-decay study of ^{12}Be. Further experimental support for this suggestion has come through measurements of transition strengths to the 1_1^- [18], 0_2^+ [19,20], and 2_1^+ bound states [21], through extraction of the ground state charge radius [22], and through nuclear knock-out [23], break-up [24,25], transfer [26], and charge exchange [27] reactions. These measurements have shown that the $N = 8$ magic number is clearly broken in ^{12}Be and the detailed mixing of the shells is still being investigated. The short lifetime combined with the narrow separation of the bound states has made it difficult to study these states individually.

^{11}Be is a well known one-neutron halo nucleus. This large separation of the ^{10}Be and the halo neutron in ^{11}Be has led to an interpretation of ^{12}Be as having a three-particle structure with a ^{10}Be core and two neutrons [28]. The 1_1^- state is particularly interesting in a three-body model. This state is only 1 MeV below the two-neutron threshold and is expected to be a two-neutron halo in the three-body model with one neutron in an s state and the other in a $p_{1/2}$ state. A fifth bound state that differs
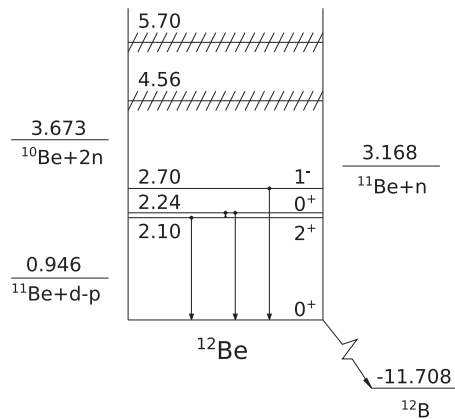

044619-1

FIG. 1. The level scheme of ^{12}Be containing the known states and resonances as well as the gamma decay transitions for the bound states. The energies are given in MeV and the values for the bound states and the resonances are taken from [18–20,34].

from the 1_1^- state only in spin coupling has been suggested: a 0_1^- state with an excitation energy around $E^* = 2.5$ MeV [29]. However, this state has never been seen experimentally.

Several other models have been used to predict the ^{12}Be structure: apart from shell models and a simple wave-function ansatz [30], antisymmetrized molecular dynamics [31], the deformed potential model [32], as well as the generator coordinate method and no core shell model [33] have all been employed.

The first studies of excited states in ^{12}Be were in transfer reactions, mainly ^{10}Be$(t, p)^{12}$Be; these results are summarized by Fortune *et al.* [34]. Most recent studies have been in break-up reactions, and also a ^{11}Be$(d, p)^{12}$Be transfer reaction has been performed at TRIUMF by Kanungo *et al.* [26]. Spectroscopic factors were determined in the latter for all four bound states. The value for the 0_2^+ state was only given with a large uncertainty, due to the inability to clearly distinguish it from the 2_1^+ state. The spectroscopic factors determined in the experiment at TRIUMF have later been questioned, since they disagreed with theoretic calculations [30].

In this paper, we report on a ^{11}Be(d, p) experiment performed at ISOLDE. The setup represents an improvement upon an earlier ^{9}Li(d, p) experiment [35] as both gamma rays and charged particles were measured, enabling a clear identification of all the bound states in ^{12}Be. Hence, detailed studies of each state have been made and spectroscopic factors have been determined for all the four states. The lifetime and the branching ratio of the decay of the 0_2^+ state have also been determined. Results from the other reaction channels as well as on the unbound resonances in ^{12}Be [36] will be reported elsewhere.

The paper starts with a description of the experimental setup and experimental procedure, Sec. II. The analysis of the data is described in Sec. III. The focus of the analysis is the identification of the individual states, but the lifetime of and the branching ratio for the decay of the 0_2^+ state are also given. The analysis is done in three steps described in Sec. III. The determined differential cross sections are presented along with the distorted wave Born approximation (DWBA) calculations

in Sec. IV. The spectroscopic factors are also presented and discussed in this section. The paper ends with a short summary and conclusion in Sec. V.

II. THE EXPERIMENTAL PROCEDURE

The experiment was performed at the ISOLDE facility, CERN, Switzerland. The ^{11}Be activity was produced by a 1.4 GeV proton beam through fragmentation of a uranium carbide target. The Be atoms were subsequently ionized via laser ionization [37], mass separated, and led to the REX-ISOLDE post-accelerator. Here they were bunched in REXTRAP, fully stripped to charge state +4 in REXEBIS, and finally post-accelerated to 2.8 MeV/u (30.7 MeV) in the REX linear accelerator [38]. The beam intensity after post-acceleration fluctuated between 4.4×10^6/s and 1×10^7/s. This led to a total number of ^{11}Be nuclei of $N_{^{11}\text{Be}} = 1.11(25) \times 10^{12}$. The beam intensity was determined by Coulomb scattering on a silver target, which was performed regularly during the experiment. The fluctuation in the beam intensity was monitored via the rate of detected particles (p, d, and t) throughout the experiment. The setup allowed for a study of several properties of the secondary ^{11}Be beam. The beam spot was determined to be a flat distribution on an area with a diameter of approximately 6 mm; details are given in [39].

A deuterated polyethylene (CD$_2$) target was used in the experiment. The thickness of the target was 1.00(5) mg/cm^2. Runs on a pure carbon target and a regular polyethylene target (CH$_2$) were performed and provided information about reactions on C and H in the primary target.

A setup specialized for transfer reaction experiments at ISOLDE was used. The setup consisted of the MINIBALL germanium detector array [40,41] in combination with the T-REX silicon detector setup [42]. The T-REX was used to detect the light charged particles from the reaction. The T-REX consisted of 12 silicon telescope detectors placed to cover angles from 8° to 152° in the laboratory and with an almost 2π-azimuthal angular coverage. A drawing of the T-REX is seen in Fig. 2(a). Figure 2(b) shows the angles and energies covered by the T-REX (grey area). The dashed lines represents the energy required for a proton to pass through the first of the telescope detectors. The kinetic curves of the four known bound states are also shown in Fig. 2(b). Particle identification through ΔE-E plots can be performed above the dashed lines. Particles with energy less than 1 MeV could not be separated from the noise level.

The gamma-ray detection provided by the MINIBALL was required to separate the bound states in ^{12}Be. The MINIBALL consists of 24 germanium detectors placed in eight clusters. The clusters were placed to cover a wide angular range. The germanium detectors had an energy range up to 8 MeV. The energy-dependent detection efficiency was determined using three gamma sources (^{152}Eu, ^{60}Co and ^{207}Bi) and gamma rays from β decay of ^{11}Be. The ^{11}Be beam used for the efficiency calculation was stopped in an aluminum foil at the target position. The detection efficiencies for decays occurring at the target position are given, for the relevant decays, in Table I. More details on the experimental procedures can be found in [43].
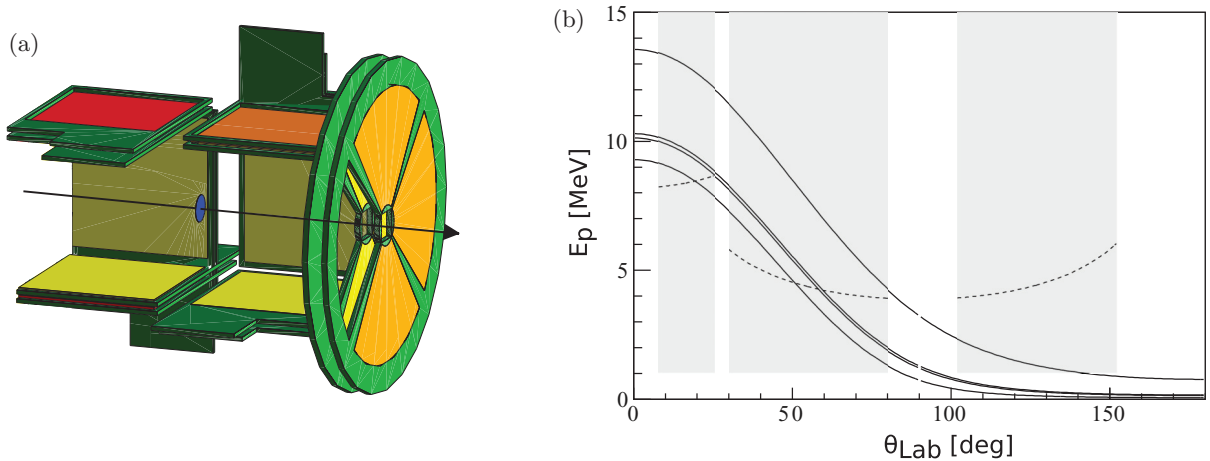
FIG. 2. (Color online) (a) A drawing of the T-REX silicon array [42]. The three detectors on the left side are omitted to clear the view inside the T-REX. (b) The kinetic curves for the emitted protons in a ^{11}Be$(d,p)^{12}$Be reaction (solid lines). Each line corresponds to a population of one of the four bound states, Fig. 1. The gray area represents the angles and energies covered by the T-REX and the dashed line corresponds to the minimum energy required for ΔE-E identification.

III. IDENTIFICATION OF THE BOUND STATES IN ^{12}BE

The identification of the four bound states in ^{12}Be is performed in three steps. The protons are identified in a ΔE-E plot if the energy of the particles is sufficiently high (Sec. III A). This is only the case for the forward laboratory angles according to Fig. 2(b). The excited states are identified using gating on gamma-ray energies afterwards. The identification of (d,p) reactions from particles stopped in the ΔE detectors is divided in two: forward and backward angles. In forward angles only protons populating ^{12}Be in an excited state will be stopped in the ΔE detector, Fig. 2(b). These protons can be identified by gating on gamma-ray energies (Sec. III C). Protons populating the ground state will have sufficient energy to penetrate the ΔE detector in the forward angle and can be ignored when analyzing particles stopped in the forward ΔE detectors. In backward laboratory angles only protons populating the ground state and particles from reactions on carbon in the target have sufficient energy to be separated from the noise level. The latter can be taken into account via the runs on a pure carbon target (Sec. III D).

A. Particles stopped in the E detector

Figure 3 shows a ΔE-E plot for one strip in one of the detectors covering the forward laboratory angles. Protons, deuterons, tritons, and α particles are easily identified. A gate

TABLE I. The γ energy and the MINIBALL detection efficiency for the four main γ-decay lines in ^{12}Be.

Decay	E_γ (keV)	ϵ (%)
$0_2^+ \rightarrow 2_1^+$	144	16.2(5)
$0_2^+ \rightarrow 0_1^+$	511 (pair creation)	8.2(5)
$2_1^+ \rightarrow 0_1^+$	2107	3.5(2)
$1_1^- \rightarrow 0_1^+$	2680	3.0(2)

is made to select the protons. Similar plots and gates have been made for each strip separately.

The excitation energy spectrum for ^{12}Be is obtained using the kinematics of the identified protons, Fig. 4(a). A large part of the protons stems from reactions on C and H in the target. The background is determined by analyzing the data from the runs on the pure carbon and the regular polyethylene target, and is indicated by the red and green lines in Fig. 4(a). Figure 4(b) shows the ^{12}Be excitation energy spectrum with the backgrounds subtracted. The ground state of ^{12}Be is clearly identified as the peak at 0 MeV. There is still a small additional background component at 1 MeV, which might extend into the ground state peak. Only the backgrounds from C and H in the target are taken into account when determining the ground state differential cross section, and the additional background will lead to an extra uncertainty in the final spectroscopic factors; see Sec. IV. The 2_1^+- and the 1_1^- states are also visible in the spectra, but the energy resolution is too poor to
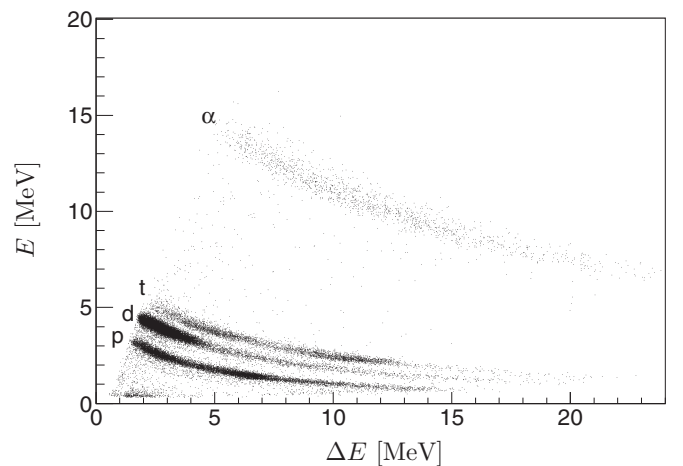

FIG. 3. A ΔE-E plot for a strip in one of the detectors covering the forward laboratory angles. The three curves corresponding to p, d, and t are clearly separated.
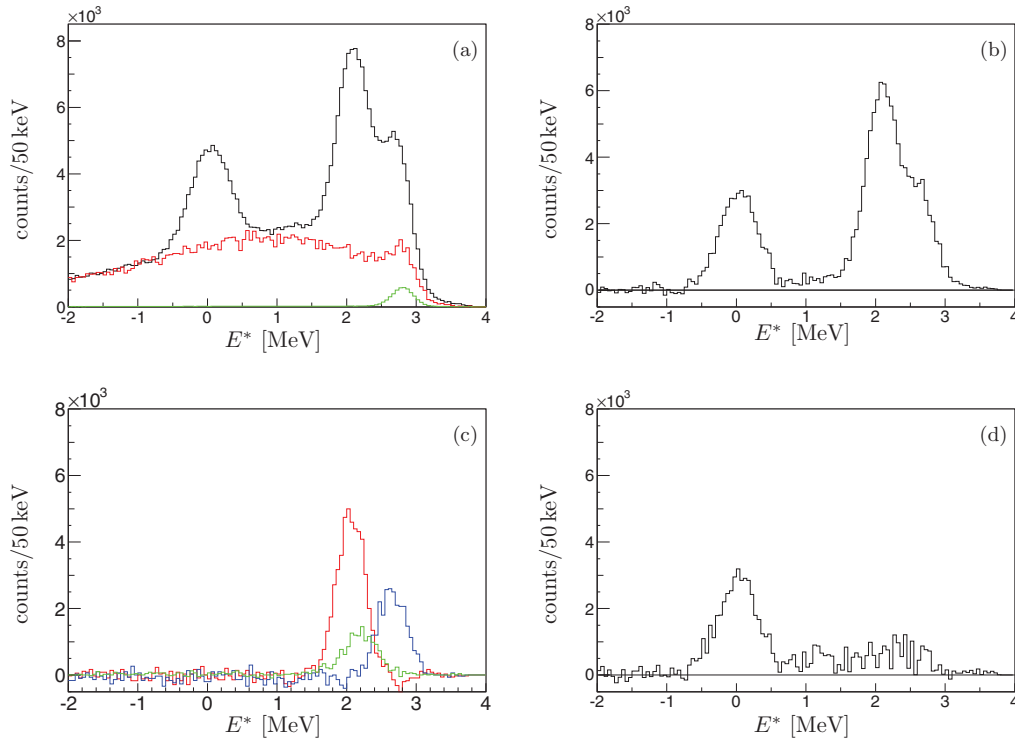
FIG. 4. (Color online) Four plots showing the excitation energy of ^{12}Be. (a) The excitation energy spectrum determined from the momentum of protons identified from the ΔE-E plots (black) along with the background spectra determined from runs on the carbon target (red or dark gray) and the CH$_2$ target (green or light gray). (b) The excitation energy spectrum from (a) with the two background spectra subtracted. (c) Excitation energy spectra determined from protons gated on the gamma lines shown in Fig. 5. Red (dark gray): 2_1^+ ($E_{\text{peak}} = 2061$ keV); green (light gray): 0_2^+ ($E_{\text{peak}} = 2190$ keV); and blue (black): 1_1^- ($E_{\text{peak}} = 2658$ keV). (d) The excitation energy spectrum from (b) with the three spectra gated on gamma rays in (c) subtracted; only the ground state peak is present.

separate the two or to see the 0_2^+ state at 2.24 MeV, and gates on gamma-ray energies are required to identify these states. Gates on the gamma-ray energies have been determined from the spectra in Fig. 5, which is described below. The gate on gamma-ray energies have been applied and the spectra for the three excited states are shown in Fig. 4(c). Figure 4(d) shows the total excitation energy spectrum with efficiency corrected background and spectra with gates on gamma-ray energies applied subtracted. This spectrum should thus represent the ground state of ^{12}Be. Only few events with $E^* > 0.6$ MeV are observed in Fig. 4(d). This shows that almost every event in the total spectrum can be described either from reactions on C and H in the target or from (d, p) reactions.

The gates used for Fig. 4(c) are determined from two spectra, Figs. 5(a) and 5(c). A gamma-ray energy spectrum is produced using gamma rays in coincidence with the identified protons, Fig. 5(a). The energy is corrected for Doppler-shift, due to the emission from a moving nucleus. Peaks at 2103 keV and at 2722 keV are clearly seen. The two peaks are from the decay of the 2^+ and the 1^- state to the ground state respectively; see Fig. 1 and Table I. Gates are set on the two peaks and excitation energy spectra of ^{12}Be are generated using protons in coincidence with gamma rays within these gates, Fig. 4(c) (red and blue). The two spectra are scaled with $1/\epsilon$ from Table I to take the MINIBALL detection efficiency into account. The two peaks are situated at 2061 ± 202 keV and

2658 ± 192 keV respectively, validating the interpretation that the protons within the gate on the gamma-ray energies stem from the population of the 2_1^+ and the 1_1^- states.

The 0_2^+ state is long lived, the lifetime of the state was determined to be $\tau = 331(17)$ ns by Shimoura *et al.* [20]. The excited ^{12}Be nuclei are either stopped within the setup or far away from the MINIBALL detectors before decaying. Only gamma rays from ^{12}Be nuclei stopped within the setup can be detected for the 0_2^+ state. The nuclei are stopped in the forward silicon detectors or in the frame holding the detectors. This require an outgoing angle larger than $7°$ for the ^{12}Be nucleus, which corresponds to center-of-mass angles between $71°$ and $122°$ for the protons. The beam width gives a probability of the reaction happening off-center, increasing the required outgoing angle of ^{12}Be for some events. This will lead to a drop in the detection efficiency for events with an outgoing ^{12}Be angle close to $7°$, leading to a larger uncertainty in the differential cross section around $70°$ and $120°$. The events populating the long lived 0_2^+ state can be identified by looking at time-delayed gamma rays. Figure 5(b) shows the time between the detected gamma rays and the detected proton (Δt) against the laboratory gamma energy. The laboratory gamma energy is used, as the gamma rays of interest come from stopped nuclei. Events with $|\Delta t| < 75$ ns are considered prompt decays and events with $\Delta t > 100$ ns are considered delayed gamma decays. The spectra in Fig. 5(c)
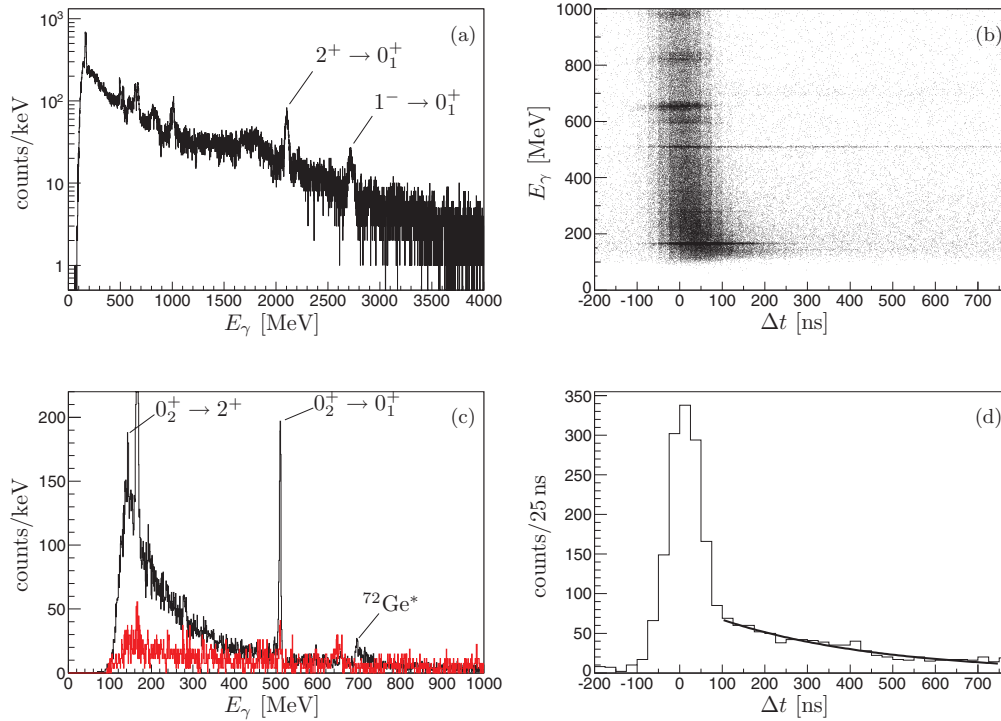
FIG. 5. (Color online) Spectra for gamma-ray energies in coincidence with identified protons. (a) Doppler-corrected energy spectrum. (b) The laboratory gamma-ray energy vs the time difference between the detected proton and the detected gamma ($\Delta t = t_\gamma - t_p$). (c) The laboratory gamma-ray energy spectrum before the reaction ($\Delta t < -75$ ns) (red or gray) and after the reaction ($\Delta t > 100$ ns) (black). (d) The time difference between the detected gamma and the detected proton for gamma rays in the peak at 509.6 keV along with the fit to an exponential decay used to determine the lifetime of the 0_2^+ state.

shows a projection onto the gamma energy axis before (red) and after (black) the reaction. A peak at 166 keV is present both before and after the reaction. The peak also appears when carbon or regular polyethylene targets are used. The fact that the peak is ever-present, even at times when no beam has hit the target, indicates that the peak stems from a background. The origin of the peak is not known, but is expected to stem from long-lived isotopes from a previous experiment. An excitation energy spectrum made with a gate on 166 keV shows a flat distribution ranging from -4 MeV to 3 MeV. This confirms the interpretation of a background peak. The reaction leads to an increase in the overall background, but three new peaks emerge after the reaction: two narrow and one broad. The mean values and widths of the three peaks are determined using a Gaussian fit: 143.5 ± 2.7 keV, 509.6 ± 2.5 keV, and 709 ± 23 keV. The first two are identified as the decays of the 0_2^+ state; see Table I. The last one stems from decay of excited ^{72}Ge within the MINIBALL detector. The germanium isotopes are excited through inelastic scattering with neutrons and decay subsequently [44,45].

The two time-delayed peaks have been used to determine the branching ratios of the two decays:

$$\mathrm{BR}_{0^+ \to 0^+} = 87.3(35)\% \qquad (1)$$

$$\mathrm{BR}_{0^+ \to 2^+} = 12.7(35)\% \qquad (2)$$

The large uncertainty on the detection efficiency of especially the 143.5 keV gamma leads to a large uncertainty in the final

result of the branching ratio. The result is consistent with the values of 82.3(15)% and 17.7(15)% determined earlier [20].

The time signal also enabled a determination of the lifetime of the 0_2^+ state using the time-difference spectrum for the 511 keV gamma line, Fig. 5(d). The spectrum is fitted to an exponential decay and gives a lifetime of

$$\tau = 357(22) \text{ ns.}$$

The value is in fair agreement with the value $\tau = 331(12)$ ns determined by Shimoura *et al.* [20].

The last peak (green) in Fig. 4(c) is made by gating on the two time-delayed gamma peaks. Again the mean value of the excitation energy peak at 2190 keV validates the two gamma peaks as stemming from the decay of the 0_2^+ state. The spectra is scaled with a factor $1/0.63$ in addition to the $1/\epsilon$ from Table I. This extra factor of $1/0.63$ stems from the additional time gate ($dt > 100$ ns). For an exponential decay with a lifetime of 357 ns, only 63% of the decays will be within the time window of [100 ns, 750 ns].

To test for the presence of other components in the total excitation energy spectrum, Fig. 4(d) shows the spectra in Fig. 4(b) with the spectra gated on the gamma-ray energies subtracted. Most of the events above the ground state have disappeared, indicating that, with the applied scaling, the spectra produced by gating on the gamma-rays can be used for cross-section calculation without any major uncertainty in the overall amplitude. A small part of the total spectrum is still unaccounted for, which most likely stems from an unaccounted
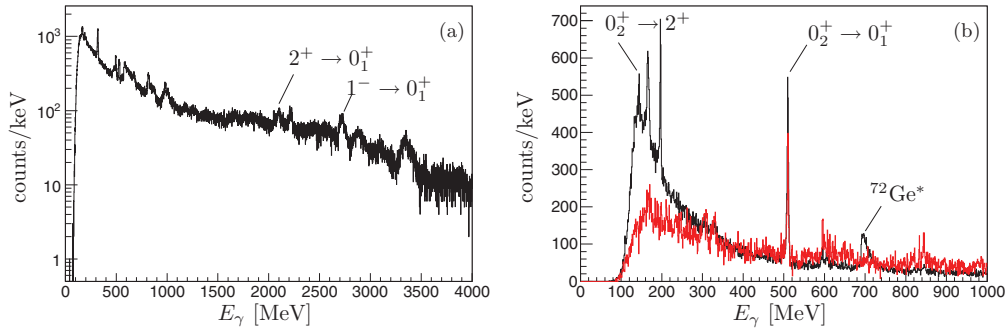
FIG. 6. (Color online) E_γ spectra for gamma rays in coincidence with unidentified charged particles stopped in the ΔE detectors. (a) Doppler-corrected energy spectrum. (b) Laboratory gamma energy spectra for gamma rays emitted before (red or gray) and after (black) the reaction. The time gates are similar to the ones in Fig. 5(c).

background, either from a small contamination of ^{22}Ne in the beam or extra contaminations in the target. The possibility of some small extra components of the three excited states can not be ruled out though. Especially the 0_2^+ state might not be fully described by the gate set on the gamma rays, due to the requirement of a stopped ^{12}Be nucleus for the gamma detection. Furthermore, the detection efficiency (ϵ) in Table I is determined for decays occurring at the target position, not in the detectors at the end of the setup, which could lead to a slight change in the scaling. Hence, the additional background leads to an extra uncertainty in the absolute amplitude of the cross sections for the two 0^+ states. This is reflected in the uncertainties of the final spectroscopic factors, Table III.

B. Search for further bound states

The extra data not accounted for by the excitation energy spectra gated on gamma rays could also stem from a yet unseen bound state in ^{12}Be. A bound 0_1^- state is predicted in a three-body model [29]. The excitation energy of the state is estimated to be between 2.1 MeV and 3.1 MeV in the model. Any 0_1^- state above the 1_1^- state can be ruled out by the data presented here. All events with excitation energy above 2.7 MeV are described by the spectra gated on gamma rays, Fig. 4(d). Furthermore, there is no gamma line between 100 keV and 400 keV in Fig. 5(a). The only peak present is the unknown background peak at 166 keV. This narrows the energy search to the interval between 2.1 MeV and 2.7 MeV. This interval can be further narrowed down. A 0_1^- state between the 2_1^+ and the 1_1^- state would mainly decay to the 2_1^+ state with an $M2$ transition. The state will then be long lived with a lifetime comparable to the 0_2^+ state. Hence a peak between 200 keV and 500 keV should emerge in the black spectrum shown in Fig. 5(c), like the 511 keV and the 143.5 keV lines. No extra peak is seen in the spectra. From this we can limit the possible energy range for a bound 0_1^- state to

$$E^* \in [2.1 \text{ MeV}, 2.2 \text{ MeV}]. \qquad (3)$$

From Fig. 4(d) we can determine the population strength for an additional state at 2.15 MeV to be more than a factor of 10 less than the 1_1^- state. This would not be the case for a 0^- state, which only differs from the 1_1^- state in spin coupling. Therefore, it is very unlikely that a bound 0^- state exists in ^{12}Be.

C. Particles stopped in the forward ΔE detector

Studying the particles stopped in the ΔE detectors is the next step. We first consider the forward laboratory angles. All protons producing ^{12}Be in the ground state go through the ΔE detector in forward angles; see Fig. 2(b). This leaves only the protons to excited states in ^{12}Be to be identified. The population of the excited states can be determined using the same gates as in the previous section. Figure 6(a) shows the Doppler-corrected gamma rays in coincidence with particles stopped in the ΔE detector and Fig. 6(b) shows the laboratory gamma energy before (red) and after (black) the reaction. The plots are similar to Figs. 5(a) and 5(c). More peaks appears in the Doppler-corrected spectrum. These gamma rays stem mainly from inelastically scattered ^{11}Be ($E_\gamma = 320$ keV), excited states in ^{10}Be populated in (d, t)-reactions ($E_\gamma = 2590$ keV, 2812 keV, and 3367 keV) and reactions on C and H. The two peaks at 2096 keV and 2723 keV are still present and easily separable from other gamma lines.

Comparing the laboratory gamma energy spectra before and after the reaction time shows the same appearance of the three peaks mentioned in the previous section. Two things should be noted. A fourth peak at 197 keV appears after the
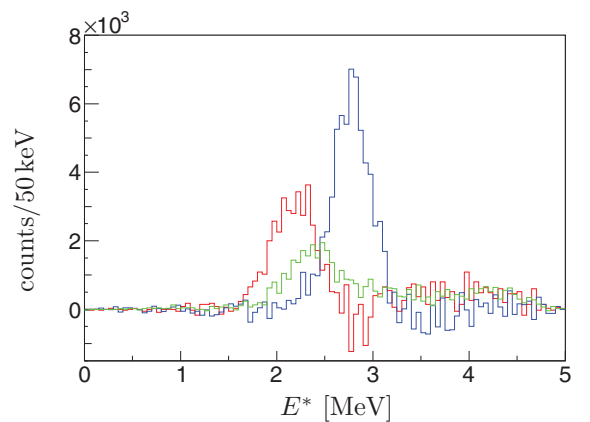

FIG. 7. (Color online) The excitation energy of ^{12}Be determined from the momentum of particles stopped in the ΔE detectors in the forward angles and gated on the gamma lines shown in Fig. 6. Red (dark gray): 2_1^+ ($E_{\text{peak}} = 2061$ keV); green (light gray): 0_2^+ ($E_{\text{peak}} = 2190$ keV); and blue (black): 1_1^- ($E_{\text{peak}} = 2658$ keV).
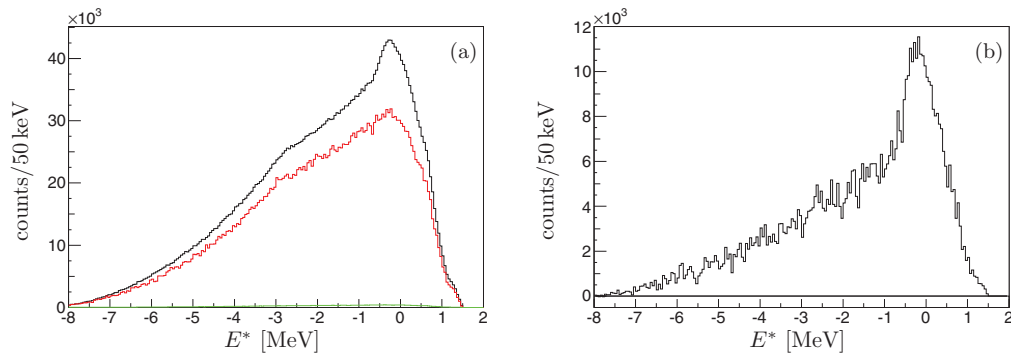
FIG. 8. (Color online) Excitation energy spectra of ^{12}Be calculated for particles in backward laboratory angles. (a) The total excitation energy spectrum (black) along with the background spectra from runs on the carbon target (red or dark gray) and the CH$_2$ target (green or light gray). (b) The excitation energy spectrum with the two background spectra subtracted.

reaction point. The peak stems from decays in ^{19}F populated in reactions of ^{11}Be on ^{12}C in the target. Secondly, a significant peak at 511 keV is seen before the reaction time. This indicates a non-negligible background from positrons within the ISOLDE experimental hall. This leads to a significant background when using the gate, which is taken into account when producing the excitation energy spectrum gating on gamma rays, Fig. 7. All three spectra produced with a gate on gamma-ray energies in Fig. 7 are peaked at the correct excitation energies, and the background which remains is negligible.

D. Particles stopped in the backward ΔE detector

The last part of the analysis concerns the backward laboratory angles. Protons producing ^{12}Be in the ground state are the only ones detected in the backward angles, due to the high lower energy detection threshold, Fig. 2(b). An excitation energy spectrum is made from all particles stopped in the ΔE detector in backward angles. All particles are assumed to be protons, Fig. 8(a). Backgrounds from C and H in the target are subtracted using the runs on pure carbon and regular polyethylene targets, Fig. 8(b). The ground state is clearly seen, but a significant background is still present. The background leads to a larger uncertainty in the determined differential cross sections for the small center-of-mass angles.

IV. RESULTS

The experimental differential cross sections for the (d, p) population of the four bound states are determined by comparing the excitation energy spectrum, determined in Sec. III, with a GEANT4 [46] simulation. This simulation was done using the G4MINIBALL package [42]. The excitation energy spectra produced using gates on the gamma-ray energies from Figs. 4(c) and 7 are used for the excited states (2_1^+, 0_2^+, and 1_1^-). The total excitation energy spectra from Figs. 4 and 8 are used for the ground states. The experimental differential cross sections are shown in Fig. 9 (dots).

Theoretical calculations of the differential cross sections are needed in order to extract conclusions from the experimental results. This step is complex in our case, partly because

the "forward peak" is only covered for the ground state transition, partly because both initial nuclei—the deuteron and ^{11}Be—are loosely bound systems. The theory for (d, p) reactions is still being refined for challenging cases like this and
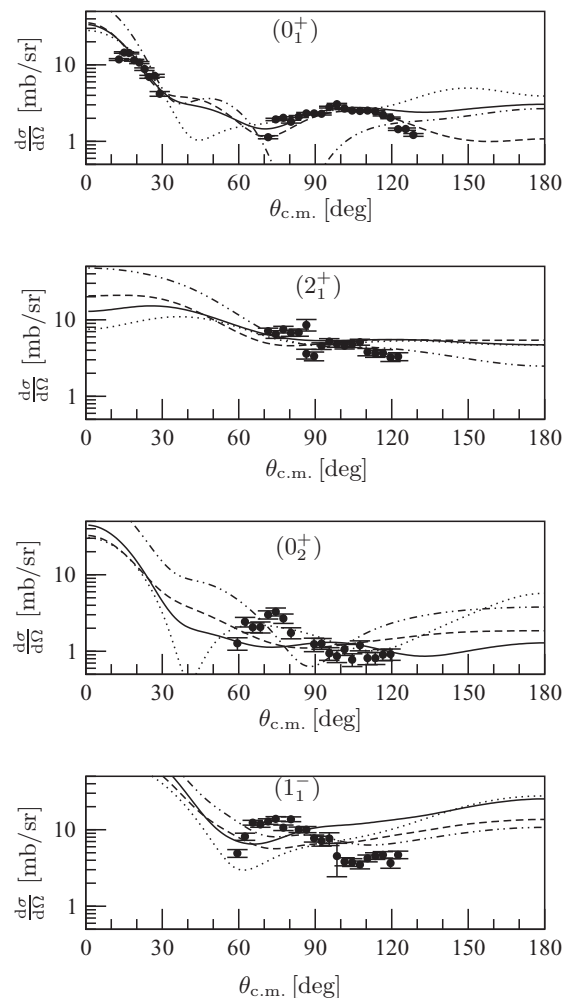

FIG. 9. The experimentally determined differential cross sections for the four bound states in ^{12}Be (dots). The DWBA calculations are plotted on top of the experimental data. set I: full line (——); II: dashed (- - -); III: dotted ($\cdots$), and IV: dash-dotted ($\cdot - \cdot$).

TABLE II. Parameters for the six optical potentials used in the four (I–IV) DWBA calculations along with the two binding potentials for ^{2}H and ^{12}Be. All potentials have a Wood-Saxon shape except the ^{1}H $+ n$ potential, which is a Gaussian shape.

Channel	Set	V_0	r_0	a_0	δ_1	δ_2	W_v	W_d	r_I	a_I	V_{so}	r_{so}	a_{so}
^{12}Be $+ p$	I + II + III	57.8	1.25	0.25	0	0	0	8.08	1.4	0.22	6.5	1.25	0.25
	IV	58.59	1.12	0.67	0	0	0.85	5.26	1.3	0.51	5.53	0.90	0.59
^{11}Be $+ d$	I	124.7	0.9	0.9	0	0	0	4.38	2.452	0.264	6.0	0.9	0.9
	II	120.18	0.9	0.9	0.84	1.27	0	19.535	2.452	0.264	6.0	0.9	0.9
	III	118.0	0.87	0.91	0	0	0	5.80	1.57	0.78	5.80	0.87	0.91
	IV	80.53	1.17	0.8	0	0	5.19	4.71	1.56	0.8	3.54	1.23	0.81
^{1}H $+ n$		72.15	1.484										
^{11}Be $+ n$		54.14	1.35	0.9							8.50	1.35	0.9

is often making use of continuum discretized coupled channel (CDCC) calculations; see [47–49] and references therein. The concept of a spectroscopic factor, often used earlier as the key quantity to be extracted from experiment, has also been questioned during the last decade—see Mukhamedzhanov [49] and Jennings [50] for recent overviews—asymptotic normalization coefficients (ANCs) [49,51–53] have been used instead. A proper theoretical analysis of our data is beyond the scope of the present paper so we shall here just briefly indicate what can be learned from a standard approach to allow comparison with earlier experimental work [26].

The differential cross sections are compared to distorted wave Born approximation (DWBA) calculations performed with FRESCO [54,55]. Four DWBA calculations are performed using the parameters from Table II. The interaction potentials are of the form

$$V(r) = -V_0 f(x_0) - i \left(W_v f(x_I) - W_d \frac{df((x_I))}{dx_I} \right)$$
$$+ V_{so} \frac{\hbar^2}{m_\pi c} \frac{1}{r} \frac{df((x_{so}))}{dx_{so}} (\vec{L} \cdot \vec{s})$$

where $f(x)$ is the Wood-Saxon potential:

$$f(x_i) = \frac{1}{1 + \exp(x_i)},$$
$$x_i = \frac{r - r_i A^{1/3}}{a_i}.$$

The ^{12}Be $+ p$ potentials are taken from Ref. [56] (set I + II + III) and [57] (set IV). The first ^{11}Be $+ d$ potential is calculated from generalized parameters given by Satchler I. [58] (set I). The depth of this potential is modified for

the second set (set II) and a deformation taken from Hussein *et al.* [59] is added. The second potential fits better the elastic scattered deuterons (not investigated here). The last two ^{11}Be potentials are taken from Fitz *et al.* [60] and Han *et al.* [61]. These two potentials were used in combination with the two ^{12}Be $+ p$ potentials to investigate the differential cross sections from the ^{11}Be$(d, p)^{12}$Be experiment performed at TRIUMF by Kanungo *et al.* [26].

The two binding potentials are taken from Austern *et al.* [62] for ^{1}H $+ n$ and Nunes *et al.* [63] for ^{11}Be $+ n$. The ^{11}Be $+ n$ potential has a Wood-Saxon shape and the ^{1}H $+ n$ has a Gaussian form:

$$V(r) = V_o \exp[(r/r_0)^2].$$

The parameters can be seen in Table II.

The theoretical differential cross sections for each of the four sets of parameters are plotted in Fig. 9. The deduced spectroscopic factors from the four calculations are given in Table III. The spectroscopic factors are given along with spectroscopic factors determined by Kanungo *et al.* [26] and from two theoretical models: a shell model calculation made by Fortune *et al.* [64] and a three-body model calculation made by Garrido *et al.* [65]. Effects of core excitation are not yet included in the three-body model [65].

The cross sections from set IV can only reproduce the shape of the 2_1^+ cross section, and the validity of these parameters is very questionable. The first three sets reproduce the ground state well and to a large extent the 2_1^+ state. Only set III can reproduce the shape for the 0_2^+ state and none of the potentials can reproduce the shape for the 1_1^- state. The low binding energy and the possible two-halo structure of the 1_1^- state are

TABLE III. Spectroscopic factors for the four bound states in ^{12}Be. The spectroscopic factors are given for each set of parameters shown in Table II along with spectroscopic factors from a ^{11}Be(d, p) experiment performed at TRIUMF [26], a shell model calculation [64], and a three-body calculation [65]. Square brackets indicate cases where the angular shapes do not match.

State	Set I	Set II	Set III	Set IV	Ref. [26]	Ref. [64]	Ref. [65]
0_1^+	$0.15^{+0.03}_{-0.05}$	$0.25^{+0.05}_{-0.08}$	$0.15^{+0.03}_{-0.05}$	$[0.30^{+0.20}_{-0.22}]$	$0.28^{+0.03}_{-0.07}$	0.78	0.60
2_1^+	0.15(5)	0.30(10)	0.075(25)	0.40(10)	$0.1^{+0.09}_{-0.07}$	0.52	(0.35)
0_2^+	$[0.40^{+0.14}_{-0.10}]$	$[0.32^{+0.12}_{-0.09}]$	$0.40^{+0.13}_{-0.09}$	$[0.95^{+0.43}_{-0.36}]$	$0.73^{+0.27}_{-0.40}$	0.37	0.07
1_1^-	[0.55(20)]	[0.50(20)]	[0.27(15)]	[0.85(35)]	≈ 0.35	–	0.50

expected to play an important role in the reaction mechanism to the 1_1^- state. The overall agreement is not satisfactory, but as mentioned above this is not too surprising, and a better description of the reaction mechanisms is needed where effects due to the halo structure of the two initial nuclei, e.g., break-up of the halo [48,66], are included. The deduced spectroscopic factors are highly model dependent as seen in Table III. Especially set IV gives values that are not consistent with any of the other sets. The validity of the values from set IV has already been questioned, due to the discrepancy in the angular shapes. The strong disagreement between sets III and IV is in contradiction with the result found in [25], where the two sets are claimed to provide consistent results. The spectroscopic factors for the excited states found by set III are consistent with the values found in [25]. For the excited 0_2^+ state the previous determination carried a large uncertainty since the 2_1^+ and the 0_2^+ states could not be separated in [25]. The states are identified and separately analyzed in this experiment, and this should provide a more reliable value for the 0_2^+ state. The factor of 2 between the two ground state values is not understood.

The experimental spectroscopic factor is, in contrast to the theoretical ones, larger in the excited 0^+ state than the ground state; this and the overall large disagreement between the experimental determined spectroscopic factors and the theoretical ones is still to be understood.

V. SUMMARY AND CONCLUSION

The combined power of the T-REX and MINIBALL arrays allows us to identify individual final states in the ^{11}Be$(d, p)^{12}$Be reaction. All previously known excited bound states have been seen through observation of gamma rays from their decay. For the decay of the 0_2^+ state the lifetime has been measured to be $\tau = 357(22)$ ns and the branching ratios of the decays to the ground state and the 2_1^+ state have been determined to be $\mathrm{BR}_{0^+ \to 0^+} = 87.3(35)\%$ and $\mathrm{BR}_{0^+ \to 2^+} = 12.7(35)\%$ respectively. These values are in good agreement with previously determined values. No indications for new bound states were seen; there are in particular no indications for the presence of a bound 0_1^- state. The excitation energy of such a bound state has been limited to be between the 2_1^+ and the 0_2^+ states in an interval of only 100 keV. The amount of unaccounted data within this interval will lead to a population

strength much below that expected for a bound 0_1^- state. Hence a fifth bound state in ^{12}Be can be ruled out.

Differential cross sections have been extracted over a large angular range ($60°$ to $120°$ in the center-of-mass system) and compared to four different sets of DWBA calculations in order to determine spectroscopic factors. None of the DWBA calculations could reproduce all of the experimental differential cross sections. The difference between the experimental and theoretical differential cross sections is large, especially for the high-lying levels. This may be due to the loosely bound neutrons in the initial states and the suggested halo structure of some of the final states, factors which are known to affect the reaction mechanism. More refined calculations must be made for the theoretical differential cross sections, e.g., Coupled-Reaction-Channels found to be essential to describe the ^{8}Li $+ ^2$H reaction at a similar energy [53]. The current disagreement between theoretical and experimental spectroscopic factors may be due to the simplicity of the DWBA calculations, but it is disturbing that the relative strength of transitions to the two 0^+ states has opposite trends for theory and experiment. It will clearly be important to go beyond the simple theoretical treatment presented here.

[1] B. Jonson, Phys. Rep. **389**, 1 (2004).
[2] A. S. Jensen, K. Riisager, D. V. Fedorov, and E. Garrido, Rev. Mod. Phys. **76**, 215 (2004).
[3] I. Tanihata, H. Savajols, and R. Kanungo, Prog. Part. Nucl. Phys. **68**, 215 (2013).
[4] K. Riisager, Phys. Scr. T **152**, 014001 (2013).
[5] W. von Oertzen, M. Freer, and Y. Kanada-Eny'o, Phys. Rep. **432**, 43 (2006).
[6] T. Baumann, A. Spyrou, and M. Thoennessen, Rep. Prog. Phys. **75**, 036301 (2012).
[7] H. Simon, Phys. Scr. T **152**, 014024 (2013).
[8] R. Kanungo, Phys. Scr. T **152**, 014002 (2013).
[9] K. Blaum, J. Dilling, and W. Nörtershäuser, Phys. Scr. T **152**, 014017 (2013).
[10] T. Aumann and T. Nakamura, Phys. Scr. T **152**, 014012 (2013).
[11] N. Keeley, R. Raabe, N. Alamanos, and J. L. Sida, Prog. Part. Nucl. Phys. **59**, 579 (2007).
[12] K. Wimmer et al., Phys. Rev. Lett. **105**, 252501 (2010).
[13] A. Bonaccorso, Phys. Scr. T **152**, 014019 (2013).
[14] K. L. Jones, Phys. Scr. T **152**, 014020 (2013).
[15] K. T. Schmitt et al., Phys. Rev. Lett. **108**, 192701 (2012).
[16] I. Talmi and I. Unna, Phys. Rev. Lett. **4**, 469 (1960).
[17] F. C. Barker, J. Phys. G **2**, L45 (1976).
[18] H. Iwasaki et al., Phys. Lett. B **491**, 8 (2000).

[19] S. Shimoura *et al.*, Phys. Lett. B **560**, 31 (2003).
[20] S. Shimoura *et al.*, Phys. Lett. B **654**, 87 (2007).
[21] N. Imai *et al.*, Phys. Lett. B **673**, 179 (2009).
[22] A. Krieger *et al.*, Phys. Rev. Lett. **108**, 142501 (2012).
[23] A. Navin *et al.*, Phys. Rev. Lett. **85**, 266 (2000).
[24] S. D. Pain *et al.*, Phys. Rev. Lett. **96**, 032502 (2006).
[25] W. A. Peters *et al.*, Phys. Rev. C **83**, 057304 (2011).
[26] R. Kanungo *et al.*, Phys. Lett. B **682**, 391 (2010).
[27] R. Meharchand *et al.*, Phys. Rev. Lett. **108**, 122501 (2012).
[28] C. Romero-Redondo, E. Garrido, D. V. Fedorov, and A. S. Jensen, Phys. Rev. C **77**, 054313 (2008).
[29] C. Romero-Redondo, E. Garrido, D. V. Fedorov, and A. S. Jensen, Phys. Lett. B **660**, 32 (2008).
[30] H. T. Fortune and R. Sherr, Phys. Rev. C **85**, 051303 (2012).
[31] Y. Kanada-En'yo and H. Horiuchi, Phys. Rev. C **68**, 014319 (2003).
[32] I. Hamamoto and S. Shimoura, J. Phys. G **34**, 2715 (2007).
[33] M. Dufour, P. Descouvemont, and F. Nowacki, Nucl. Phys. A **836**, 242 (2010).
[34] H. T. Fortune, G.-B. Liu, and D. E. Alburger, Phys. Rev. C **50**, 1355 (1994).
[35] H. B. Jeppesen *et al.*, Nucl. Phys. A **748**, 374 (2005).
[36] E. Garrido, A. S. Jensen, D. V. Fedorov, and J. G. Johansen, Phys. Rev. C **86**, 024310 (2012).
[37] V. N. Fedoseyev, G. Huberg, U. Köster, J. Lettry, V. I. Mishin, H. Ravn, and V. Sebastian, Hyperfine Int. **127**, 409 (2000).
[38] O. Kester *et al.*, Nucl. Instrum. Methods Phys. Res. Sect. B **204**, 20 (2003).
[39] J. G. Johansen, M. A. Fraser, V. Bildstein, T. Kröll, R. Raabe, K. Riisager, D. Voulot, and K. Wimmer, Nucl. Instrum. Methods A **714**, 176 (2013).
[40] J. Eberth *et al.*, Prog. Part. Nucl. Phys. **46**, 389 (2001).
[41] N. Warr *et al.*, Eur. Phys. J. A **49**, 40 (2013).
[42] V. Bildstein *et al.*, Eur. Phys. J. A **48**, 85 (2012).
[43] J. G. Johansen, Ph.D. thesis, Aarhus University, 2012 (unpublished), CERN-THESIS-2012-282.
[44] C. Chasman, K. W. Jones, and R. A. Ristinen, Nucl. Instrum. Methods **37**, 1 (1965).
[45] D. G. Jenkins *et al.*, Nucl. Instrum. Methods A **602**, 457 (2009).
[46] S. Agostinelli *et al.*, Nucl. Instrum. Methods A **506**, 250 (2003).
[47] N. Keeley, N. Alamanos, and V. Lapoux, Phys. Rev. C **69**, 064604 (2004).
[48] A. M. Moro, F. M. Nunes, and R. C. Johnson, Phys. Rev. C **80**, 064606 (2009).
[49] A. M. Mukhamedzhanov, Phys. Rev. C **84**, 044616 (2011).
[50] B. K. Jennings, arXiv:1102.3721.
[51] A. M. Mukhamedzhanov and R. E. Tribble, Phys. Rev. C **59**, 3418 (1999).
[52] N. K. Timofeyuk, R. C. Johnson, and A. M. Mukhamedzhanov, Phys. Rev. Lett. **91**, 232501 (2003).
[53] E. Tengborn *et al.*, Phys. Rev. C **84**, 064616 (2011).
[54] I. J. Thompson, Comput. Phys. Rep. **7**, 167 (1988).
[55] I. J. Thompson and F. M. Nunes, *Nuclear Reactions for Astrophysics* (Cambridge University Press, Cambridge, 2009).
[56] J. R. Comfort and B. C. Karp, Phys. Rev. C **21**, 2162 (1980).
[57] A. J. Koning and J. P. Delaroche, Nucl. Phys. A **713**, 231 (2003).
[58] G. R. Satchler, Nucl. Phys. **85**, 273 (1966).
[59] M. S. Hussein and R. Lichtenthäler, Phys. Rev. C **77**, 054609 (2008).
[60] W. Fitz, R. Jahr, and R. Santo, Nucl. Phys. A **101**, 449 (1967).
[61] Y. Han, Y. Shi, and Q. Shen, Phys. Rev. C **74**, 044615 (2006).
[62] N. Austern *et al.*, Phys. Rep. **154**, 125 (1987).
[63] F. Nunes *et al.*, Nucl. Phys. A **609**, 43 (1996).
[64] H. T. Fortune and R. Sherr, Phys. Rev. C **83**, 044313 (2011).
[65] E. Garrido *et al.* (unpublished).
[66] A. M. Moro and R. Crespo, Phys. Rev. C **85**, 054613 (2012).